

The Calice Analog Scintillator-Tile Hadronic Calorimeter Prototype

M. Danilov

Institute of Theoretical and Experimental Physics, Moscow, Russia and

G. Eigen

University of Bergen, 5007 Bergen, Norway

(representing the Calice collaboration)

An analog scintillator-tile hadron calorimeter prototype is presently under construction by members of the Calice collaboration. This highly-granular 38-layer calorimeter is designed to test the calorimetric aspect of the particle flow concept. The scintillation light is collected with wavelength-shifting fibers attached to SiPMs. A preamplifier with two gain settings allows us to measure both single pixels and up to 100 MIPs. We have monitored the quality of more than 5000 SiPMs and have performed the first radiation hardness studies. We developed a calibration and monitoring system that is based on LEDs distributing UV light via clear fibers to each tile. We have also tested the first completed layers with cosmic muons and positrons. First tests in a hadron beam will start at CERN in July 2006.

1. INTRODUCTION

The physics requirements at the International Linear Collider (ILC) impose high demands on the performance of calorimeters. The ultimate goal is to achieve a jet-energy resolution of $30\%/\sqrt{E}$, in order to obtain excellent separation of WW events from ZZ events and to increase the sensitivity for reconstructing Higgs bosons and supersymmetric particles. Monte Carlo studies have indicated that this goal may be achievable by utilizing the concept of particle flow, in which minimum-ionizing particles, charged hadrons, electromagnetic shower and neutral hadrons are identified separately. This requires electromagnetic (ECAL) and hadronic (HCAL) calorimeters with high granularity both in the transverse and longitudinal directions. To test this idea experimentally, appropriate ECAL and HCAL prototypes need to be built that measure large amounts of electromagnetic and hadron showers in test beams. One approach for the hadron calorimeter is the analog scintillator-tile design on which we focus in this short note.

Based upon the experience gained with a small technical prototype [1], a 1 m^3 analog hadron calorimeter prototype is presently under construction at DESY. It will be tested together with an ECAL prototype and a tail catcher. The physics objective is to accumulate a library of hadron showers over a wide range of energies (6-200 GeV) and for different incident angles. One key issue is how well two neighboring showers can be separated in this geometry, since for jet-energy measurements it is important to isolate neutral hadron showers from charged hadron showers. The beam test data will help to optimize shower reconstruction algorithms and to tune the Monte Carlo simulation. The technical aspects include the operation and calibration of about 8000 Silicon Photomultipliers (SiPM), the operation of an LED-based calibration and monitoring system and the development detailed Monte Carlo simulations.

2. THE CALICE ANALOG HADRON CALORIMETER PROTOTYPE

The analog hadron calorimeter prototype is a 38-layer sampling calorimeter made of a plastic-scintillator steel sandwich structure with a lateral dimension of about $1 \times 1\text{ m}^2$. Each layer consists of 2 cm thick steel absorber plates and a plane of 0.5 cm thick plastic scintillator tiles housed in a steel cassette. A scintillator plane or module is shown in Figure 1. For the first 30 layers, the tile sizes vary from $3 \times 3\text{ cm}^2$ for 10×10 tiles in the center of the module, to $6 \times 6\text{ cm}^2$ in the intermediate region (4×24 tiles) and $12 \times 12\text{ cm}^2$ (4×5 tiles) in the outer ring. In the last eight layers, the granularity is decreased to $6 \times 6\text{ cm}^2$ in the central region due to financial reasons. Each tile has a wavelength-shifting (WLS) fiber that is inserted into a groove and that is coupled to a SiPM on one end via an air gap. To increase the light yield, the other fiber end is covered with a mirror (3M reflector foil). In the small tiles, the grooves have a quarter-circle shape, while those in the other tiles have a full-circle shape. The sides of each tile are matted functioning as diffuse reflector. The tile faces are covered with a 3M super reflector foil.

The signal of each tile is amplified by a charge-sensitive preamplifier that is switchable between two gains in the range of 1 mV/pC to 100 mV/pC. The high gain is needed to resolve individual pixels in the calibration mode, while the low gain ascertains that energies up to 100 MIPs can be measured. After shaping in a shaping amplifier the signal is digitized in a 16-bit ADC. In the high-gain mode, a short shaping time of 40 ns is used to keep the noise contribution small. In the low-gain operation, the shaping time needs to be increased to 180 ns due to the beam trigger electronics. The readout electronics was produced by the Orsay group [2]. A VME-based data acquisition system produced by the UK Calice group [3] is used to collect and store the data.

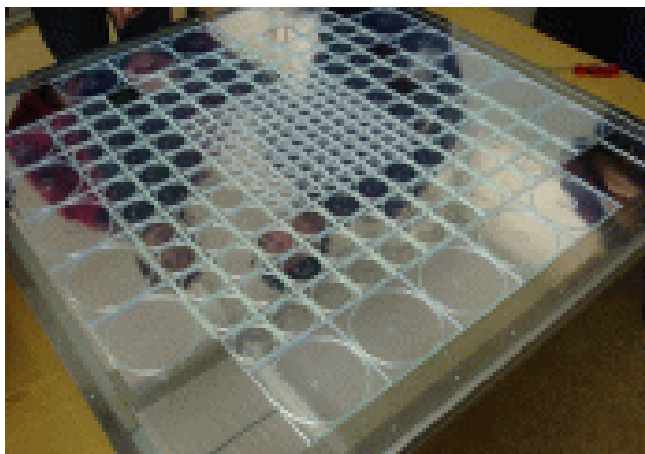


Figure 1: Tile layout of a scintillator module for layers 1-30.

The prototype consists of 7608 cells and has a thickness of 4.6 interaction lengths. It will be placed on a movable platform that allows to rotate the prototype with respect to the beam axis.

3. SiPMs FOR CALORIMETRY

A SiPM is a multipixel avalanche photodiode that is operated in the Geiger mode [4]. The detectors used for this prototype are manufactured in Russia. Enlarged photographs of an entire detector and the pixel structure are presented in Figure 2. The physical size of the entire detector is $1.5 \times 1.5 \text{ mm}^2$. The photosensitive area is $1 \times 1 \text{ mm}^2$ and holds 1156 pixels, of which each is about $20 \mu\text{m}$ wide. SiPMs are reversely biased with a voltage of $U \sim 50 \text{ V}$ producing gains of the order of 10^6 . Once a pixel is fired it triggers the Geiger discharge. The analog information is obtained by summing up the number of fired pixels. So the dynamic range for photon signals is about three orders of magnitude. Each pixel has a quenching resistor of the order of a few $\text{M}\Omega$ built in, which is necessary to break off the Geiger discharge. The recovery time is less than 100 ns per pixel. Our SiPMs are insensitive to magnetic fields as magnetic-field studies have shown [4]. Due to the Geiger mode operation, SiPMs have a negligible nuclear counter effect.

3.1. Test results of SiPMs

Currently, more than 5000 SiPMs have been produced by the PULSAR enterprise together with the CALICE MEPhI group and have been tested at ITEP in Moscow. The tests are performed in an automatic setup, where 15 SiPMs are simultaneously illuminated with calibrated LED UV light. During the first 48

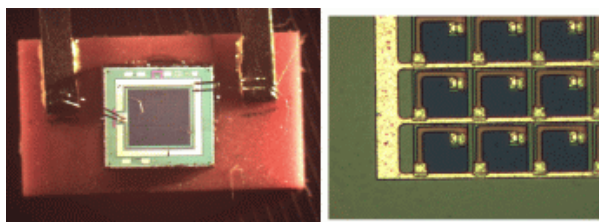


Figure 2: Photograph of a SiPM (left) and an enlargement of the pixel structure (right).

hours, the SiPMs are operated at an increased reverse-bias voltage, that is about 2 V above the normal operation voltage. Next, gain, noise and relative efficiency with respect to a reference photomultiplier are measured as a function of reverse-bias voltage. The reverse-bias voltage working point is chosen as the one that yields 15 pixels for a MIP-like signal provided by the calibrated LED.

At the working point, we measure several SiPM characteristics. With low-light intensities of the LED, we record single-pixel spectra that are used for gain calibrations. A typical single-pixel spectrum is shown in Figure 3, in which up to 9 individual pixels are clearly visible. We record the response function of each SiPM over the entire range (zero pixel to saturation). Figure 4 shows for 4000 individual SiPMs the number of fired pixels versus the light intensity in units of MIPs. The shape of the response function of all SiPMs is similar and individual curves all lie within 15%. In addition, we measure the noise rate at half a MIP threshold, the cross talk and the SiPM current. Here, cross talk denotes the effect that a Geiger discharge in one pixel triggers the firing of one or more neighbor pixels. Figure 5 shows the noise rate distribution. The arrow at 1.8 kHz shows the selection cutoff. Figure 6 depicts the cross talk distribution. The horizontal axis shows the probability for such an occurrence. The cutoff value here lies at 0.35. Figure 7 shows the current distributions. Basically, all SiPMs have values below the $2 \mu\text{A}$ cutoff.

3.2. SiPM Radiation Hardness and Aging Studies

First radiation hardness tests of SiPMs have been performed in Moscow using a proton beam of the ITEP synchrotron. Figure 8 shows the increase in SiPM current with the accumulated dose of 200 MeV protons. The current increase is compatible with that observed in other Si detectors [5]. SiPMs, however, are more sensitive to radiation damage than other Si detectors because of the high amplification ($\sim 10^6$) and a very small initial noise of about 0.1 photoelectrons. These two properties are important for a clear separation of signals with different numbers of detected photons as seen in Figure 3. This advantage which is

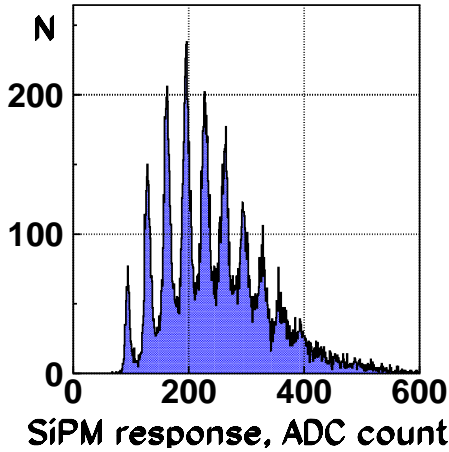


Figure 3: A typical SiPM spectrum for low-intensity light, showing up to nine individual pixels.

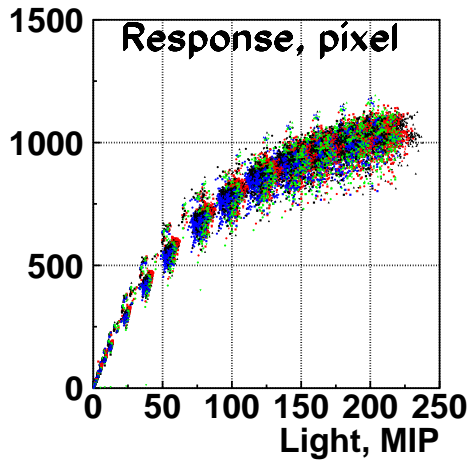


Figure 4: The response function for 4000 SiPMs.

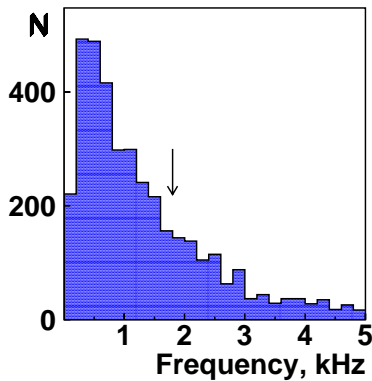


Figure 5: The noise distribution of SiPMs at half a MIP threshold.

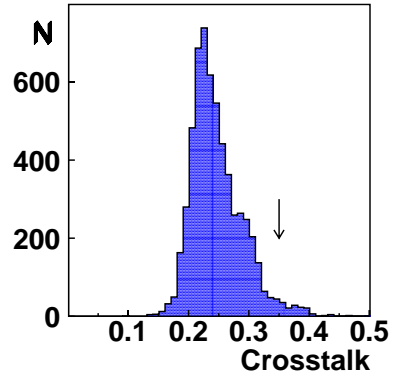


Figure 6: The cross talk distribution of SiPMs.

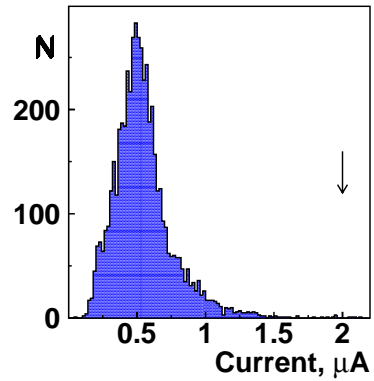


Figure 7: The current distribution of SiPMs.

important for calibration is lost after an irradiation of about 1 krad, because individual pixel peaks cannot be resolved any longer due to smearing. Nonetheless, SiPMs can be still operated even after radiation doses much larger than 1 krad, but they have an increased noise. For example, after a radiation dose of 5 krad they have an equivalent noise of about two pixels in a 50 ns wide gate. Since our MIP signals are 15 pixels on average, the additional noise of two pixels does not increase the width of the Landau distribution and thus does not influence the detection of MIPs.

The radiation hardness of SiPMs is sufficient for operations in a hadron calorimeter at the ILC. Only in the endcaps close to the beam pipe, one can expect a neutron flux above $10^{10}/\text{cm}^2/500 \text{ fb}^{-1}$, which would lead to excess currents above $5 \mu\text{A}$ and thus cause a smearing of individual pixel peaks. We have assumed here a standard energy-dependent relative radiation damage efficiency of neutrons and protons [5]. Future tests will study the effect of long-term low-dose irradiation on the aging.

We have operated about 650 SiPMs for 180 days with the high voltage turned on 50% of the time. Dur-

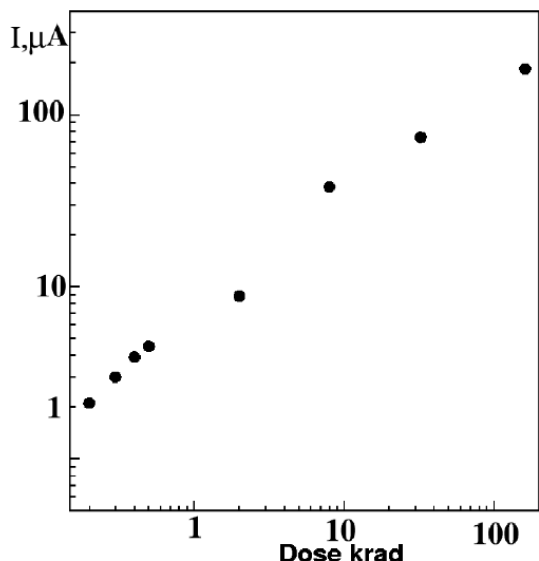


Figure 8: The SiPM current as a function of radiation dose for 200 MeV protons.

ing the first three weeks of operation the noise rate increased in six SiPMs, but they still can be operated. After the initial turn-on period, the system remained stable and no new problem appeared.

3.3. Measured Light Yield of the Scintillator Tiles

In order to cover the full dynamic range but still reveal a clear signal above noise, the minimum ionization peak (MIP) of a cell should lie in the 10-20-pixel range. So SiPMs that pass the selection criteria are installed into scintillator tiles with WLS fibers. For each tile the MIP response is measured using triggered electrons from a ^{90}Sr source. The mean value of the MIP response varies from tile to tile because of the different light collection efficiency. For a sample of 407 tiles read out with SiPMs, a mean value of 16.6 pixels was measured with a variation of about 15%.

4. SYSTEM CALIBRATION

The signal of each tile is stored in ADC bins. In order to determine the pixel gain, the amplifiers are operated in high-gain mode (calibration mode), while for the energy measurements of beam particles the amplifiers are operated at low gain (physics mode). The measured energy A in units of ADC bins is

$$A[\text{ADC}] = A_{obs} - A_{ped}, \quad (1)$$

where A_{obs} is the recorded position of the signal and A_{ped} is the position of the pedestal. The pixel

gain in units of ADC bins is obtained from the peak position of the first pixel (A_{pix}) in calibration mode with respect to the pedestal

$$G[\text{ADC}/\text{pixel}] = A_{pix} - A_{ped}. \quad (2)$$

The calibration of the pixel gain is performed with low-intensity LED light. Figure 9 shows a typical SiPM calibration spectrum for 40 ns shaping. With knowledge of the SiPM response function $f_{resp}(N_{pix})$ we can determine the number of photoelectrons from the observed pixels

$$N_{pe} = f_{resp}(N_{pix}). \quad (3)$$

In the physics mode, we calibrate the ADC in units of MIPs. The amplifier is operated at low gains with a shaping time of 180 ns. The MIP peak is produced by 3 GeV positrons. A typical spectrum is displayed in Figure 10. In order to correlate the calibration mode with the physics mode, we use monitoring of LED signals in the high-gain and low-gain regions (see chapter 5). The intercalibration factor between the low-gain and high-gain modes is simply,

$$I_{phys}^{calib} = \frac{A_{LED}^{calibration}}{A_{LED}^{physics}} [\text{pixels}/\text{MIP}]. \quad (4)$$

The light yield of the MIP peak in units of pixels is obtained by

$$LY [\text{pixel}] = \frac{A_{MIP}}{G} \times I_{phys}^{calib}, \quad (5)$$

where A_{MIP} is the MIP position in units of ADC bins. At DESY, an average light yield of 13 pixels was measured with a spread of ± 2 pixels. This is a little lower than the results obtained in Moscow. The difference is consistent with operations at slightly different temperatures. The light yield in units of photoelectrons is obtained by conversion of $LY [\text{pixel}]$ with the response function. To express the energy of each cell in units of GeV, we need to convert the number of ADC bins. This involves the SiPM response function and conversion factors for pixels to ADC counts, MIPs per photoelectrons and GEV per MIP. The measured and the simulated energies are related by

$$E = \frac{f_{res} \left(\frac{A[\text{ADC}]}{A_{MIP}} \times \frac{A_{MIP}}{G[\text{ADC}/\text{pixel}]} \times I_{phys}^{calib} \right)}{f_{res} \left(LY \left[\frac{\text{pixel}}{\text{MIP}} \right] \right)} \times E_{MIP}^{MC}, \quad (6)$$

where E_{MIP}^{MC} is the mean energy in units of GeV that a minimum ionizing particle is expected to deposit in our sampling geometry.

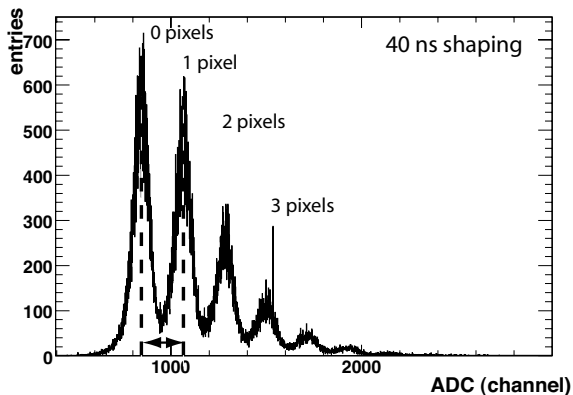


Figure 9: A typical SiPM spectrum of a scintillator tile in the calibration mode using prototype electronics.

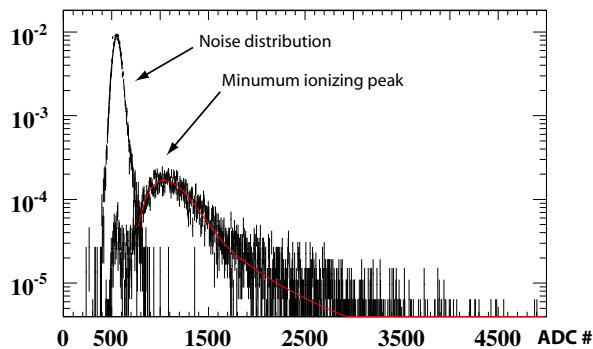


Figure 10: The energy spectrum of a scintillator tile for 3 GeV positrons showing a clear MIP peak.

5. THE CALIBRATION-MONITORING SYSTEM

It is important to monitor the stability of the entire readout system (scintillator, WLS fiber, SiPM, preamplifier and readout electronics) between MIP calibrations. In particular, we need to monitor the gain of the SiPMs, the SiPM response at a fixed LED intensity, the SiPM voltages and the temperature. This is achieved with an LED/fiber system that distributes UV light from an LED via clear fibers to each tile. 19 fibers are coupled to one LED, of which 18 fibers distribute light to 18 tiles and one fiber is read out by a PIN diode to monitor the LED light output. Thus, each HCAL plane is equipped with 12 LEDs that illuminate all 216 tiles and 12 PIN diodes that monitor the light stability of each LED. The light output of all fibers in one HCAL plane has been measured. For a fixed LED intensity, the light illuminating the tiles lies within a factor of two between maximum and min-

imum intensities. This is sufficient for all our calibration and monitoring tasks. The low-intensity spectra of all channels clearly display the typical multiple pixel peaks that are well separated from the pedestals. In addition, the SiPM response function is measurable over the entire range.

6. TEST BEAM STUDIES

One completed HCAL scintillator layer (module) was tested at DESY with 2-6 GeV positrons. To simulate the effect of electromagnetic shower evolution, lead blocks with a thickness of one radiation length (X_0) and $5 X_0$ were placed in front of the module layer. A beam trigger was defined by a coincidence of two finger counters. In order to compare the performance of the cells in the module with a reference, three plastic-scintillator counters read out with photomultiplier tubes (PMT) were installed. The first counter (dimensions: $5 \times 5 \times 0.5 \text{ cm}^3$) was placed upstream, the second counter (dimensions: $3 \times 3 \times 1 \text{ cm}^3$) was positioned right after the Pb block and the third counter was located just behind the HCAL plane (dimension: $3 \times 3 \times 1 \text{ cm}^3$). The beam was steered at the center of a tile. For the energy measurement, the signal of the center tile plus the signals of all eight neighbor tiles was used. This 3×3 array contains 99% of the lateral energy spread. 25 such arrays were studied. To reduce systematic effects from beam energy spreads, the measurements are correlated with the results of the second reference counter.

6.1. Beam Test Results

The energy reconstructed in the 3×3 array is compared to that in reference counter 2. For measurements of 3 GeV e^+ with $1X_0$ Pb, the spectrum of the center tile peaks around ~ 5 MIPs. In addition, a peak at 1 MIP is visible. The neighboring tiles show the typical tail of energy leakage on top of the noise distribution. The ratio of energy measured in the center tile and that of reference counter 2 is $r_c = 1.09 \pm 0.05$. Including the entire 3×3 array the ratio increases to $r_{3 \times 3} = 1.25 \pm 0.06$. The mean values are in good agreement with the results of MC simulations.

Figure 11 shows the measured shower shape for the setup with $5X_0$ Pb. The three histograms shown respectively with increasing amplitudes are the energy sum of the neighboring tiles, the energy of the center tile and the energy sum of center tile plus neighboring tiles. In the spectrum for the center tile, the SiPM saturation is visible. Figure 12 shows the shower energy measured in units of MIPs as a function of beam energy for the 3×3 array and for the second and third reference counters. After saturation correction in the

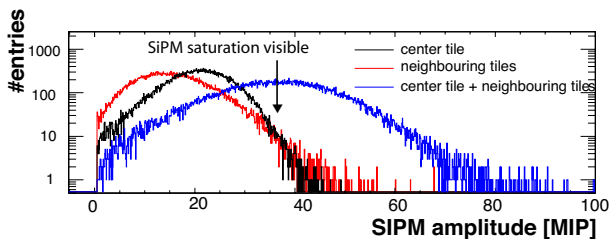


Figure 11: The shower shape in a prototype module for 3 GeV e^+ after $5X_0$. Left, middle and right distributions show energy depositions in the eight neighboring tiles, in the center tile and in all nine tiles, respectively

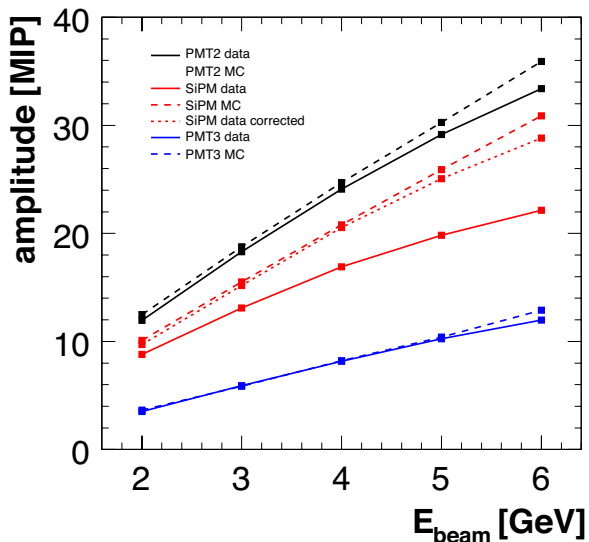


Figure 12: Measured shower energy of e^+ beam in units of MIPs versus beam energy. Solid curves show the measured distributions, dashed curves the corresponding Monte Carlo simulations and the dotted curve shows the SiPM data after saturation correction. The set of curves with increasing slopes show the results for third reference counter, the SiPM and the second reference counter, respectively.

SiPM the results are in good agreement with the MC estimate. For energies above 4 GeV, lateral energy leakage that is missing in the simulation becomes non negligible.

6.2. Results from the Cosmic Run

Three HCAL layers were also tested with cosmic muons for two weeks. Monitoring with low-intensity LED light revealed that it is important to correct the

data for temperature-dependent gain changes. The measurements yield gain changes of $dG/dT = (-1.6 \pm 0.5)\%/K$, which is in excellent agreement with the MEPHI measurement of $-1.7\%/K$. The analysis of the muon MIP distribution is in progress.

7. CONCLUSION

The construction of the analog HCAL prototype is well under way. More than half of the SiPMs have been produced and tested. First radiation hardness tests look fine for ILC applications. For low dose individual pixels can be resolved, while for a dose below 8 krad of proton irradiation the SiPM are still operable. All tiles have been produced and tested. 3080 tiles were also tested with a SiPM mounted. Presently, eight HCAL modules have been assembled at DESY and are operational, another three modules are under construction. All cells are equipped with LED monitoring. A calibration procedure has been established and successfully tested.

By July, we expect to have about 16 modules ready for the first hadron beam test, that will begin end of July at CERN. The beam test will be carried out together with an ECAL prototype and a tail catcher. By the end of 2006, we expect a completion of the entire prototype. Further tests with the full prototype with hadron beams are expected for next year at Fermilab.

Acknowledgments

We like to thank the Calice collaboration for support, in particular E. Garutti, M. Groll and F. Sefkow for helpful discussions. This work has been supported by the Norwegian Research Council and by the Russian grants RFBR 04-02-17307, SS-1722.2003, 02.445.11.7226 and ISTC grant 3090.

References

- [1] V. Andreev *et al.*, NIM A540 (2005) 368.
- [2] S. Manen *et al.*, physics/0501063 (2005).
- [3] P.D. Dauncey, hep-ex/0211052 (2002).
- [4] G. Bondarenko *et al.*, NIM A 442 (2000) 187.
- [5] G.Lindstrom NIM A512 (2003) 30.